K. KARIMI
C. CRUA
M R. HEIKAL
*E M. SAZHINA**
ICEG, School of Engineering, University of Brighton, UK

Split Injection Strategy for Diesel Sprays: Experiment and Modelling

An experimental programme to characterise Diesel fuel sprays was conducted in a Proteus high-pressure rapid compression machine (RCM), at Sir Harry Ricardo Laboratories at University of Brighton. The Proteus experiments aimed to simulate realistic Diesel engine working conditions whilst allowing visualisation of in-cylinder processes by various optical and laser diagnostics techniques. The spray penetration was explored by laser diagnostics methods such as Laser Induced Fluorescence (LIF) and the Mie scattering techniques. High-speed video (HSV) images of the spray were also recorded to show the temporal evolution of the spray. Both liquid and vapour phases of the spray were captured by the LIF technique whilst Mie scattering only recorded the liquid part of the spray. In the current study, a 7-hole injector of the solenoid type was injecting 20mm^3 of Diesel fuel each cycle at an injection pressure of 100MPa and in-cylinder pressures 2MPa and 6MPa. The fuel was injected in a split mode with various dwells between the 10mm^3 + 10mm^3 splits (or individual fuel injections). The instantaneous injection rate was measured by the long-tube rate technique. These data were taken as an input to the numerical model tracking the centre-of-mass (CoM) of the injected fuel. The modelling is based on the conservation of momentum of injected fuel mass in the presence of a realistic drag force acting on the whole spray as a physical body. This approach is particularly suitable for the dense sprays near the nozzle as an asymptotic case for the strong interaction between the spray droplets. Hence the CoM approach is seen as complementary to the traditional Lagrangian modelling for dispersed sprays widely employed by Computational Fluid Dynamics (CFD) codes. Air entrainment was modelled by the exponential decay of liquid fraction in the spray with a characteristic time τ. *Under the conventional assumption of the conical shape of the spray, the penetration of spray tip was associated with the height of the cone. This allowed the calculation of the frontal area A required in the expression for the drag force. The numerical CoM model was validated against the experimental CoM data in the range of in-cylinder pressures and dwells between two consecutive injections (or splits). The following four cases were calculated and validated against the experimental data: in-cylinder pressures (ICP) 2MPa and 6MPa, split injection strategy with dwells 0.425ms and 0.625ms between injections. In all cases, the injection pressure was 100MPa; under cold intake conditions of ambient air. For validation purposes the image processing software was extended to characterise the position of the centre-of-mass of injected fuel. The ratio of tip penetration to the position of the centre-of-mass,* β *was assessed from LIF images for ICP = 2MPa and dwells 0.425ms and 0.625ms. An average value of the ratio with a corresponding standard deviation* $\beta = 1.85 \pm 0.3$ *was accepted for the validation of the model calculations versus experiment for all cases under consideration. An uncertainty corridor was constructed for the model validation against the HSV experiment. The corridor was formed by the curves corresponding to* $\beta = 2.15$ *and* $\beta = 1.55$ *with the curve for* $\beta = 1.85$ *in the middle. A good agreement was observed between the calculated and experimental CoM penetration. The same set of modelling parameters including spray dispersion time* τ *= 0.15ms was taken by the model for all the cases under consideration.*
Key words: diesel spray penetration, split injection, multiple injection

Nomenclature

A	Projected frontal spray area
C_D	Drag coefficient for the whole spray
$\dot{m}_f$	Mass flow rate of fuel injection
Re_{in}	Reynolds number based on the initial value of fuel injection velocity and nozzle diameter
s_{tip}	Position of spray tip or spray penetration length
s	Position of centre-of-mass (CoM) of injected fuel or spray CoM penetration length
t	Time from the first sighting of fuel in the engine cylinder
t_{OD}	Opening delay (time taken from injection trigger to the first sighting of fuel through the nozzle)
u_{inj}	Injection velocity
u_{tip}	Spray tip velocity
u	Velocity of CoM of the spray
V	Volume of spray including both injected fuel and entrained air

Greek Symbols

β Empirical estimate of the ratio of spray tip penetration to the position of Centre-of-Mass (CoM)

ρ_g In-cylinder gas density.

ρ_l Liquid fuel density.

Acronyms

CFD Computational Fluid Dynamics
CoM Centre of Mass of the injected fuel mass
ICEG Internal Combustion Engine Group of School of Engineering, University of Brighton
ICP In-Cylinder Pressure
HSV High-Speed Video
LIF Laser Induced Fluorescence
RCM Rapid Compression Machine
TDC Top Dead Centre
VCO Valve Covered Orifice

1. Introduction

In-cylinder spray formation and penetration are important phenomena that constitute the foundation for a good combustion performance of a Diesel engine. The onset of combustion is preceded by spray break-up, droplet evaporation, and mixing of fuel vapour with in-cylinder charge (physical ignition delay) followed by the chemical ignition delay due to chemical mechanism of autoignition (Sazhina et al, 2000). Combustion performance and the level of exhaust emissions are dependent upon the quality and timing of the fuel spray emerging from the injector nozzle.

The characteristics of the fuel spray are dependent upon many parameters such as injection pressure, in-cylinder pressure and temperature, type of injector; number of nozzle holes and nozzle hole sizes. It is helpful to distinguish the effects of fuel injection equipment (FIE) on spray formation from the influence of in-cylinder processes. In what follows, these two tasks of the study will be referred to as FIE Characterisation (FIEC), and In-Cylinder Characterisation (ICC). The paper describes the experimental programme accomplishing both tasks for the cases under study, of high pressure Diesel sprays in a realistic engine environment.

FIEC Task: For the characterisation of the FIE, the conventional long-tube rate of injection technique was applied. This technique allowed instantaneous measurements of rate of injection (Karimi et al, 2006; Baniasad, 1994; Bosch, 1996)

ICC Task: For characterisation of a Diesel fuel spray penetration rate, methods of direct imaging based on laser diagnostics were applied (Crua, 2002; Kennaird *et al,* 2002).

Section 1 will describe the capabilities and setup of the dedicated equipment of ICEG for the study. Section 1.1 will describe long-tube injection rate experiment for achieving the FIEC goals; Sections 1.2 – 1.4 will outline the setup and capabilities of laser-diagnostics techniques on *Proteus* RCM that are used for accomplishing the ICC Task. A comparative analysis and critical assessment of the results for the experimental cases under consideration will be performed in Section 2.

The study will focus on the split injection strategy that has proved beneficial for simultaneous reduction of NOx and soot in Diesel engines (Lee and Park, 2003; Tow *et al*, 1994; Pierpont *et al*, 1995).

Modelling of transient penetration of individual injected portions of fuel under split injection strategy is a particularly challenging task that will be undertaken in Section 3 of the paper. The modelling will be based on a novel approach for tracking the CoM of the fuel injected at each split.

1. Description of the ICEG Experimental Capabilities and Setup

The extensive experimental facilities of Sir Harry Ricardo Laboratories, within the ICEG (http://www.brighton.ac.uk/iceg/), enable detailed experimental studies of Diesel sprays under novel injection strategies. The experiment for the FIEC task will be discussed below. In-cylinder diagnostics will described in subsequent sections.

1.1 Measurements of rate of injection by the Long-Tube Technique

The long-tube technique allows the measurement of instantaneous mass flow rate (Lucas 1995; Baniasad, 1994). A pair of strain gauges measuring variation in the internal pressure is fitted to the tube immediately downstream of the injector nozzle outlet (Fig 1).

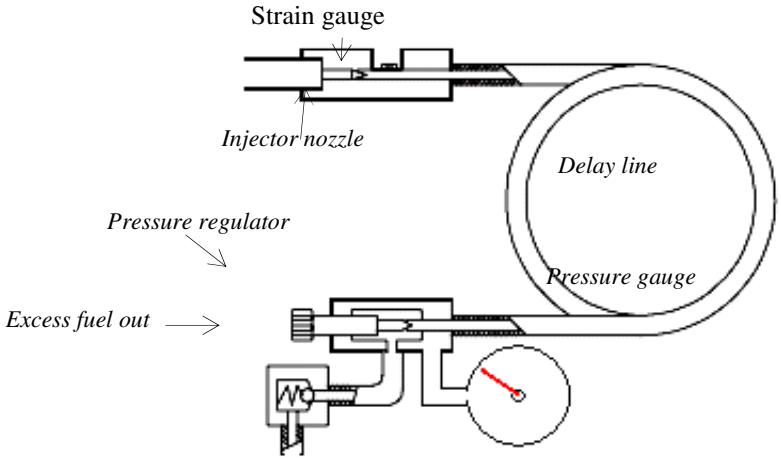

Fig 1. Schematic diagram of the long-tube

It can be shown that the strain gauge signal is proportional to the rate of injection (Lucas, 1995; Bosch, 1996). Knowing the amount of fuel injected, the observed transient profile can be calibrated or normalised, thus giving transient mass flow rate profile, $\dot{m}_f(t)$. The injection velocity can be assessed from it for a given liquid fuel density and nozzle area. For all traces, an average of 100 cycles was recorded and compared with instantaneous recordings to ensure repeatability.

1.2 *Proteus* Spray Rig

The *Proteus* is a single cylinder two-stroke rapid compression machine, with a specially designed head for optical access for spray visualisation (Fig 2). The optical head of the Proteus was designed to result in near quiescent air conditions in the spray chamber with a maximum predicted local air velocity of 1 $m.s^{-1}$ in order to avoid disturbance of the spray development by the air motion, as well as to achieve maximum loop scavenging efficiency in the combustion chamber. In addition, this design has the added advantage of allowing the study of the air entrainment created by the emerging liquid spray itself. The spray chamber within the optical head was cylindrical, and had dimensions of 50mm in diameter, and 80mm in height. This allowed sufficient space for the spray to develop without any wall impingement. As a result of the spray chamber cavity forming the top of the combustion chamber the compression ratio is only 9:1. This is too low compared to real engines; the way realistic pressures are achieved is by pressurising and heating the intake air before it enters the cylinder. Two pressure transducers were fitted to the engine combustion chamber. The first was a water cooled Kistler 6061 fitted to the optical head to monitor the in-cylinder gauge pressure with a range of 0-20 MPa. The second pressure transducer was a Kistler 4045-A10 with a range of 0-1 MPa fitted just above one of the inlet ports in the combustion chamber to monitor the absolute boost pressure. The *Proteus* engine was coupled to a DC dynamometer via reduction belts (6:1). With an operating speed of 3000 rpm at the dynamometer, a corresponding engine operating speed of 500 rpm at the flywheel was reached.

A second generation common rail fuel injection system was used to generate the injection pressures ranging from 60 to 160 MPa. The fuel pump was driven externally via an electrical motor running at 1400 rpm to maintain the required high pressure in the fuel rail with minimum fluctuation. Under the current study, the injector used was a 7-hole, 0.135 mm diameter VCO injector, operating at 100MPa injection pressure.

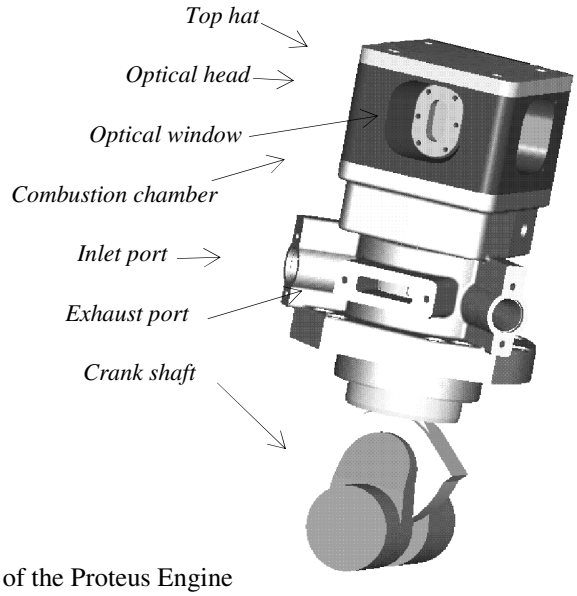

Fig 2. CAD drawing of the Proteus Engine

1.3 High-Speed Video (HSV) Image Acquisition System

A Phantom V7.1 high-speed camera was used for spray visualisation. The camera featured an 8-bit monochromatic CMOS sensor, and a global electronic shutter that allowed exposures down to $2\mu s$. Two 125 W halogen flood lights fitted with diffusers were used as shown in Fig 3, each one focused on the fuel spray axis from opposite sides.

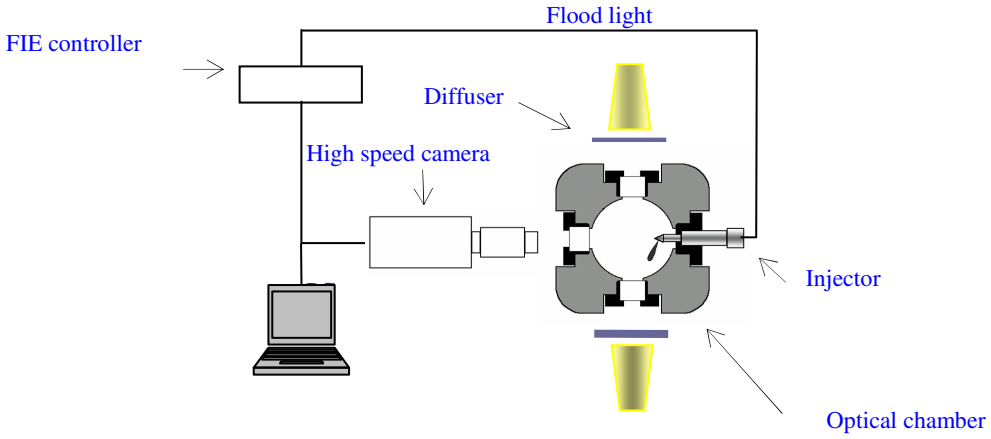

Fig 3. Schematic diagram of the experimental set-up for HSV spray imaging.

The processing of the video images for measurement of the spray penetration was performed by purpose-developed software (Crua, 2002). Suitable pixel thresholding was carried out in order to pick out the tip of the spray farthest from the nozzle.

1.4 Description of LIF and Mie imaging techniques

The laser used in the current experiment was a pulsed Nd:YAG capable of delivering pulses up to 300 mJ of energy, at a frequency of 10 Hz. The beam was tuned to 266 nm, it had a diameter of 8.7 mm and a pulse duration of 6 ns (FWHM), the laser pulses were spatially and temporally Gaussian.
The acquisition was done with a CCD camera featured with a resolution of 1280 x 1024 pixels, pixel size of 6.7 x 6.7 µm, a dynamic range of 12 bit, and a sensitivity range from 290 to 1100 nm. However, due to the use of an image intensifier, the overall spectral range of the final image will be affected. The selected lens for the camera was UV grade

and had a 105 mm focal length.
An image-doubling adapter was fitted onto the lens in order to simultaneously record the laser-induced fluorescence (LIF) and Mie scattering signals (Fig 4). The filter for the LIF signal had a high transmittance between 300 and 450 nm and blocked the scattering at 266 and 532 nm. A bandpass filter centred on 532 nm was used for the Mie scatter, along with a neutral density filter to reduce the relatively high intensity of the signal.

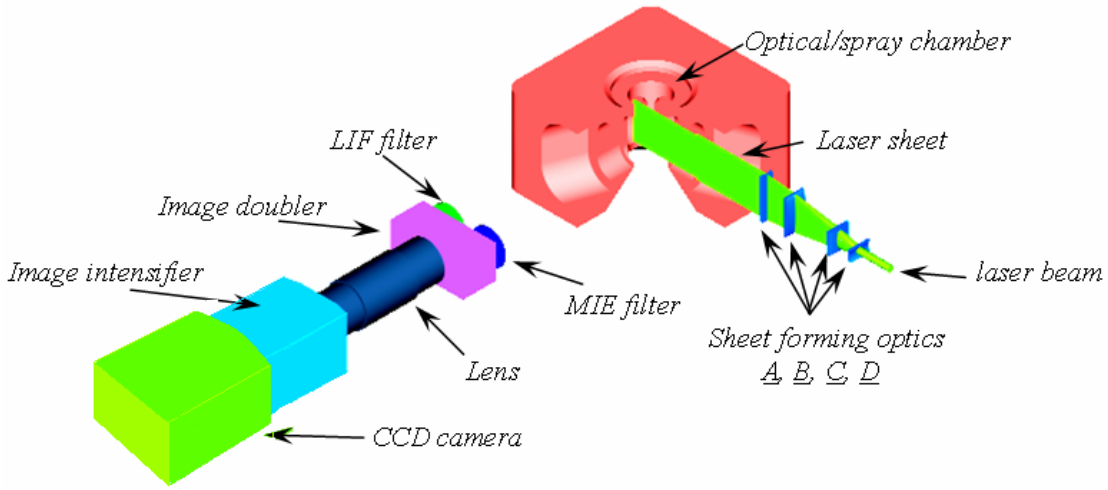

Fig 4. Schematic of the optical Proteus spray chamber, the intensified camera, and laser sheet

For the cold air intake, image acquisition was carried out every 10 µs, and every 30 µs for the hot air intake, throughout the duration of the injection. For each time step, 15 images were recorded to take into account cycle-to-cycle variation. A purpose built software package extracted the spray tip penetration and dispersion angle for the LIF and Mie signals.

2. Comparative analysis of the LIF, Mie and HSV experimental results

As it was described above, the *Proteus* RCM is a powerful tool for studying spray formation and penetration by various optical methods. A comparative analysis of the results obtained by all three techniques is quite important for assessing the reliability of experimental data. It should be expected that the results may differ due to the nature of visualisation; namely, LIF will give the tip of fuel penetration both in vapour and liquid phases; the Mie and HSV techniques will show the tip of penetrating liquid fuel even if it broke into several blobs (so-called cluster shedding). Thus the spray structure could be qualitatively assessed through the comparison of images. Each technique has its own level of image thresholding and the resulting image is averaged over individual spray events. This makes the comparison of all three techniques a challenging and interesting task. In what follows, the results of the comparison are presented for the cases under consideration.

The spray tip penetration as obtained experimentally by all these three techniques, is shown below for two cases, ICP = 2MPa and ICP = 6MPa. The density of liquid fuel at 300K is 838kgm^{-3}. Both cases are for injection pressure 100MPa and cold intake of ambient air.
The fuel was injected under split injection strategy. The first and second injected portions of fuel (or splits) were equal in size, (10mm^3 + 10mm^3), and the end of the first injection was separated by the interval of time (or dwell) of about 0.425ms injection from the beginning of the second split (Case1 and 2, see Table 1).
The same operating conditions but with the dwell of 0.625ms was investigated by the present study for comparison (Case 3 and 4, see Table 1). The experimental mass flow rate injection profile for the given injector at 100MPa injection pressure is shown in Fig 5.

Table 1. Summary of cases under consideration: in-cylinder temperature (K) and pressure (MPa) are shown at TDC when the spray is injected. Injection pressure is 100MPa and cold intake of ambient air for all cases.

	TDC Pressure, MPa	TDC Temperature, K	Density, kg.m^{-3}	Dwell, ms
Case 1	2	350	19.9	0.425
Case 2	6	448	46.7	0.425
Case 3	2	350	19.9	0.625
Case 4	6	448	46.7	0.625

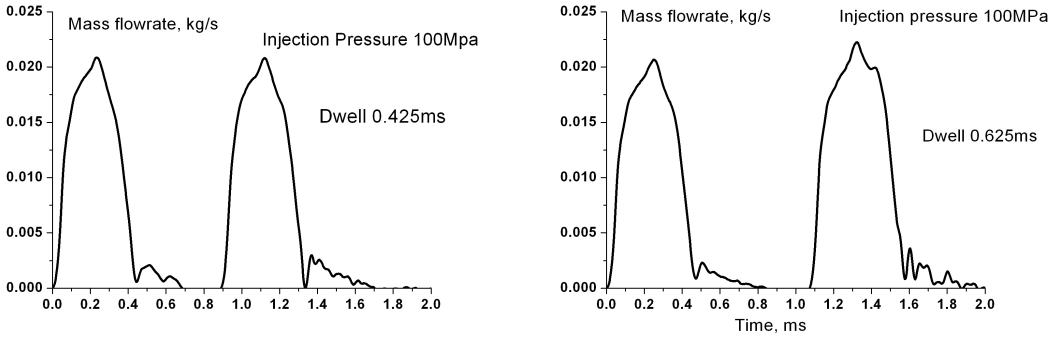

Fig 5 Transient injection mass flow rate obtained in the long-tube experiment for the injection pressure 100MPa, a) dwell 0.425ms; b) dwell 0.625ms.

The injection velocity was calculated from the measured transient mass obtained by the long-tube rate by assuming that the nozzle hole is fully opened. Cavitation effects may cause a reduction in the effective nozzle area up to a factor of 0.6. Hence the assumption of a fully-open nozzle area corresponded to the lowest injection velocity that could be obtained for a given mass flow rate profile. This added some uncertainty to the experimental data on injection velocity and subsequent modelling.
Regarding the study of spray after the exit from the injector (ICC task), the LIF, Mie and HSV images were obtained with high time resolution: $5\mu s$ increments for LIF and Mie images, and $29\mu s$ for the HSV images. The spray tip penetration was calculated from the images using a custom-built programme.
The results are compared in Fig 6a for ICP = 2MPa, and Fig 6b for ICP = 6MPa, dwell 0.425ms in both cases.

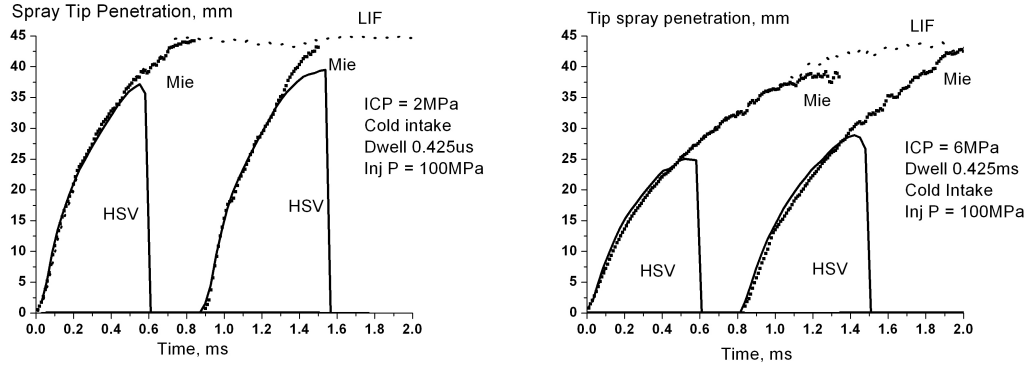

Fig 6 a, b. Transient spray tip penetration for injection pressure 100MPa, dwell 0.425ms, a) ICP = 2MPa;
b) ICP = 6MPa as obtained by three experimental techniques, LIF (upper curve, dotted), HSV (solid curves, the lowest ones in the plot).The Mie results are shown by the middle curves. The optical access window does not allow viewing spray penetration when it exceeds 45mm.

As can be seen from Fig 6, all three curves almost coincide until *t= 0.5ms* where *t* is the time from the first sighting of fuel from the nozzle. It can be concluded that the evaporation is small at this interval of time because the LIF curve (tracking vapour and liquid) practically coincides with the Mie and HSV plots The Mie curve also coincides with the HSV curve in the range 0.8 - 1.3ms for the second split. This could be expected as both of them show liquid part of the spray. The LIF curve shows higher penetration in this range corresponding to the fuel vapour of the first fuel portion (first split). It should be pointed out, however, that the LIF data are not reliable enough in this range because the optical access window does not allow spray penetration exceeding 45mm to be viewed. The divergence of the Mie and HSV curves at 0.5ms and 1.45ms can be attributed to the onset of high dispersion of the spray. The agreement between the three experimental techniques is quite significant for confirming reliability and robustness of the experimental data. Hence it is concluded that they could make a good benchmarking tool for modelling.

3. Modelling the position of Centre-of-Mass (CoM) of injected fuel

Highly dense fuel sprays in the vicinity of the nozzle exit constitute a challenge for the traditional Lagrangian tracking approach. It is based on the assumption that liquid volume fraction in the spray is small, and the drag force on the

droplets is accounted for solely by the interaction with the gas. Hence an alternative approach is sought for the case of a dense spray when the interaction between the droplets is dominant. A modelling approach to dense spray penetration based on tracking the centre-of-mass (CoM) of the injected fuel is described below. This is seen as an asymptotic case for a dense spray at the early stages of injection. It aims to complement the conventional Lagrangian tracking of individual droplets (or droplet parcels) which are more suitable for a dispersed spray (Sazhin *et al*, 2001; Sazhin *et al*, 2003).

3.1 Formulation of the model for CoM tracking

A modelling approach for a dense spray is sought from first principles. This is an approach based on the conservation of momentum when applied to the whole spray as a physical body. The equation for momentum conservation for the total injected mass of fuel can be written for quiescent in-cylinder gas as

$$\frac{d(mu)}{dt} = \rho_l \, A_n \, u_{inj}^2 \, - \frac{1}{2} C_D \, \rho_g \, A \, u_{tip}^2 \qquad (1)$$

where C_D is the drag coefficient for the whole spray (as opposed to a droplet) , A is the frontal spray area, u_{tip} is the tip velocity of the spray, and u is the velocity of centre of mass (CoM) of the spray.

The model takes the transient experimental mass flow rate profile $\dot{m}_f(t)$ as an input into the calculations. In equation (1), m is the instantaneous mass of spray; this is total injected fuel mass at a given moment of time calculated from the conservation of mass as: $m \equiv m(t) = \int_0^t \dot{m}_f dt$

An extension to the software processing the LIF images was made enabling the calculation of the position of centre-of-mass (CoM) of injected fuel from an image. The pixel intensity is proportional to local volume fraction of fuel under the LIF technique. It was used as a weighting factor during the calculations. The images were processed for Cases 1 and 3 in Table 1. The ratio of spray tip penetration to centre-of-mass penetration β is calculated at each time step for Cases 1 and 3. No systematic dependency of β with time, and from case-to-case, is observed when analysing the data. Hence an average value of β over time, and across both cases, is accepted for further analysis.

The spray tip velocity and the CoM velocity are linked by taking time derivative of $s_{tip} = \beta s$; for a constant value of β it can be concluded that the tip velocity $u_{tip}(t)$ can be replaced by $\beta u(t)$ in (1). This gives:

$$\frac{d(mu)}{dt} = \rho_l \, A_n \, u_{inj}^2(t) \, - \frac{1}{2} C_D(t) \, \rho_g \, A(t) \, \beta^2 u^2 \, . \qquad (2)$$

where $u \equiv u(t)$.

The drag coefficient C_D for the spray as a bluff deformable body in the presence of air entrainment and droplet stripping is quite difficult to evaluate. For our parametric study the approach developed by Mulholland *et al.,* 1988 will be employed. They expressed the drag coefficient in an ensemble of droplets as a function of droplet spacing. For a very dense spray (when the spacing between droplets tends to zero) they used the expression for drag on a rod given as $C_D = 0.7555/Re_{in}$ where the Reynolds number, Re_{in} is based on the value of the rod diameter and its velocity (Levich, 1962). For our study, this expression for the drag coefficient on the spray immediately after the start of injection will be employed. The initial Reynolds number Re_{in} will be taken equal to 1.0 for all cases under consideration (see Table 1). The first measurement of the injection velocity has much experimental uncertainty and hence an empirical value of Re_{in} is used. This is a modelling parameter defining drag on the spray at the start of the injection The maximum value of the drag coefficient for the spray is assumed to be equal to $C_D = 1.54$. This value is given by Liu & Reitz (1993) for a deformable droplet. A linear variation of the drag coefficient is assumed between these two values in our parametric study. Thus, the expression for the drag coefficient as a function of penetration length $s \equiv s(t)$ becomes:

$$C_D = \frac{0.755}{\mathrm{Re}_{in}} + \left(1.54 - \frac{0.755}{\mathrm{Re}_{in}}\right)\left(\frac{s}{s_b}\right) \quad (3)$$

where s_b is the modelling parameter corresponding to the penetration length when the drag coefficient becomes close to that of a large deformable blob. It is taken as $s_b = 15mm$ for all the cases in Table 1. An additional condition $C_D = \min(1.54, C_D)$ is imposed in the model.

The drag force is augmented by air entrainment and hence the projected frontal spray area *A(t)* in (2) should account for this. It is assumed that the liquid fraction in the spray defined as $\varepsilon = \frac{m(t)}{\rho_l V(t)}$ decreases with time exponentially from the initial value of $\varepsilon_0 = 1$. The expression for the liquid fraction as a function of time can be written as

$$\varepsilon(t) = \varepsilon_0 \exp(-\frac{t - t_{OD}}{\tau}) \quad (4)$$

where ε is the liquid fraction in the spray, $\varepsilon_0 = 1$ is the liquid fraction in the spray before the commencement of injection process, and τ is the characteristic decay time. The opening delay t_{OD} is a characteristic of an injector. For a given injector, it is about 0.4ms; this is the time from the start of electrical signal to the injector needle to the first sighting of fuel in the engine cylinder.

The volume occupied by the spray consists of injected fuel and entrained air and it can be derived from (4) as

$$V(t) = \frac{m(t)}{\rho_l \varepsilon(t)} \quad (5)$$

It is traditional to associate the spray shape with a cone at the early stages of penetration before the onset of cluster shedding. Following this conventional assumption, the height of the cone at each time step is assumed to be equal to the calculated spray tip penetration. This gives the expression for the volume of the spray cone as $V(t) = \frac{1}{3} A(t) \beta s(t)$. Since the spray volume is given by (5) for any moment of time, this allows to calculate the frontal area at each timestep as:

$$A(t) = \frac{3}{\beta s(t)} \frac{m(t)}{\rho_l \varepsilon(t)} \quad (6)$$

Equations (2 - 6) constitute a closed model with a tunable modelling parameter τ. A Fortran code is written for the model. Equation (2) is integrated numerically by Euler method giving the velocity $\boldsymbol{u}$ of CoM of spray for each time step. Once the value of velocity is obtained, the penetration of CoM for the injected fuel mass can be assessed by numerical integration over time.

It should be emphasised that the model takes as input only the FIE data obtained by the long-tube rate experiment (see Fig 5) and it is producing spray tip penetration for various operating conditions such as ICP and dwells between the splits. The output of the model is the transient CoM penetration length $s(t)$. Tip penetration can be estimated as $s_{tip}(t) = \beta s(t)$ for the known value of β.

The model, therefore, can be considered as a useful tool for providing spray tip penetration data from a simple rate tube test. The predictions of the model are validated against the available experimental data below, for the same value of modelling parameters Re_{in}, s_b and τ for all cases under consideration. This should help to assess the predictive abilities of the model with a view to its applications to spray penetration estimation what constitutes an important practical task.

Under current implementation, the model tracks both splits (injection portions) in exactly the same manner. The start of the second split (or start of the injection of second fuel portion) is recognised by the code as the condition when injection velocity is zero at the previous time step, and it has a non-zero positive value at the current time step. This time is taken as the new start time for the second split in the spray dispersion relation (4).

It should be kept in mind that the LIF images track both splits as a continuous monotonic curve corresponding to the penetration of the vapour cloud tip, see Fig. 6. Thus the model lends itself to the comparison with either Mie or HSV data. Both of these experimental techniques produce two spray penetration curves, one for each split.

In what follows the model will be validated against HSV and Mie data of CoM penetration, using the value of β estimated from the LIF images. This is an acceptable approach when keeping in mind a very close agreement of HSV, Mie and LIF data for the early stages of penetration.

3.2 Model validation against the experiment

The LIF images track both liquid and vapour phases and hence they give a continuous curve for the tip of the vapour penetration for both splits (both injected portions of fuel) as can be seen in Fig. 6. Hence the LIF images carry little information about the interaction between the first and second portion of fuel while it has much practical interest for a correct modelling of subsequent mixing and combustion processes.

On the other hand, the plots by HSV and Mie scattering clearly demonstrate two ascending curves corresponding to the penetration of liquid for both splits. The HSV data are selected for further analysis while the value of ratio $\beta = \frac{s_{tip}}{s}$ of spray tip to the CoM position is estimated based on the LIF image processing. This approximation is possible due to a good agreement between the predictions by all three techniques for the initial stage of spray penetration, as can be seen in Fig 6.

The value of β is taken equal to the average value of $\beta = 1.85 \pm 0.3$ over the two cases processed by the customised software, Cases 1 and 3, see Table 1. An accompanying standard deviation assesses the uncertainty corridor for the model validation against the experiment.

The plots for the experimental CoM position are shown in Fig 7 as three curves marking the uncertainty corridor for the model validation. The middle curve (solid) corresponds to the experimental data for HSV spray tip position when divided by $\beta = 1.85$. Two additional curves, dashed and dotted, correspond respectively to the division of the HSV tip data by $\beta = 1.85 + 0.3 = 2.15$ and by $\beta = 1.85 - 0.3 = 1.55$. The model predictions are considered to be satisfactory if the calculated curve (shown by open circle symbols) lies within the uncertainty corridor. The calculations were performed for the following values of parameters: $Re_{in} = 1.0$; $s_b = 15mm$ and $\tau = 0.15ms$. These values were kept the same for all the cases under consideration.

As can be seen from Fig 7, the model gives a reasonable agreement with the experimental penetration data for the dwell of 0.425ms. The agreement for the second split for ICP = 6MPa gives a slightly worse agreement for the later stages of spray penetration. This can be attributed to the effects of interaction of the tip of the second split with the tail of the first split. It could be expected that this effect is more pronounced for shorter penetration lengths and shorter dwells. This explains the model underprediction for ICP = 6Mpa and dwell 0.425ms. This case has the shortest dwell and penetration when compared with the rest of the cases under consideration in Table 1.

As can be seen from Fig 7, the calculated curves lie within the uncertainty corridor in all cases. For validation purposes, the method was applied to the same injector and operating conditions but for different value of dwell 0.625ms. The results can be seen in Fig 8a, b when compared with the HSV experimental data.
Bearing in mind the uncertainty involved in the experimental estimation of β the agreement of the model with the experiment is quite good. It should be observed that the same value of modelling parameters, namely $\tau = 0.15ms$, $\mathrm{Re}_{in} = 1.0; s_b = 15mm$ were used for all the cases under consideration, thus showing the versatility of the CoM model.

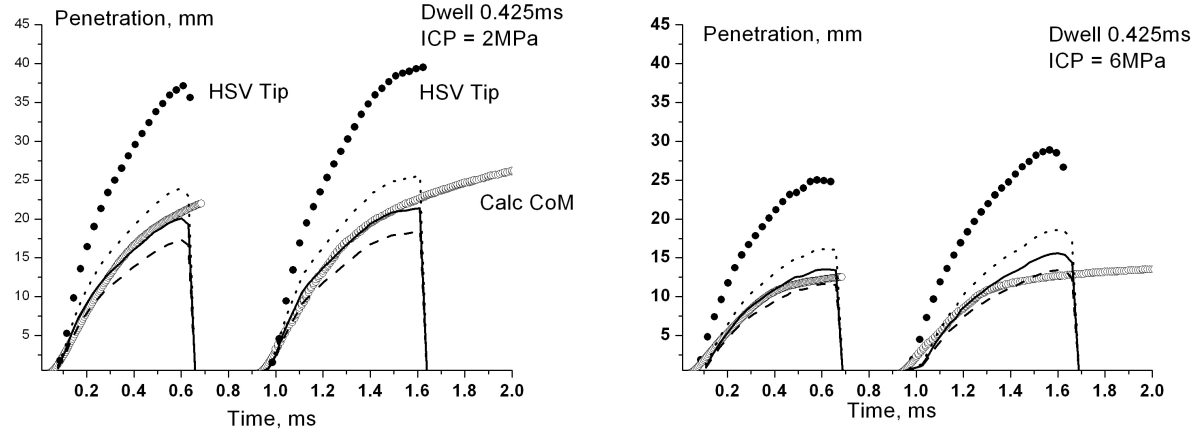

Fig 7a, b. Comparison between model predictions shown by symbols (○) , and experimental HSV results for a 0.135 mm diameter, 7-hole single VCO nozzle, at 100 MPa injection pressure cold intake, and a) ICP = 2 MPa, b) ICP = 6MPa. The symbols ● correspond to the HSV experimental data for liquid tip penetration. The experimental estimate of CoM position is shown as dashed-dotted curves forming the uncertainty corridor centred around the HSV tip penetration divided by the average value of $\beta = 1.85$ (solid curve).

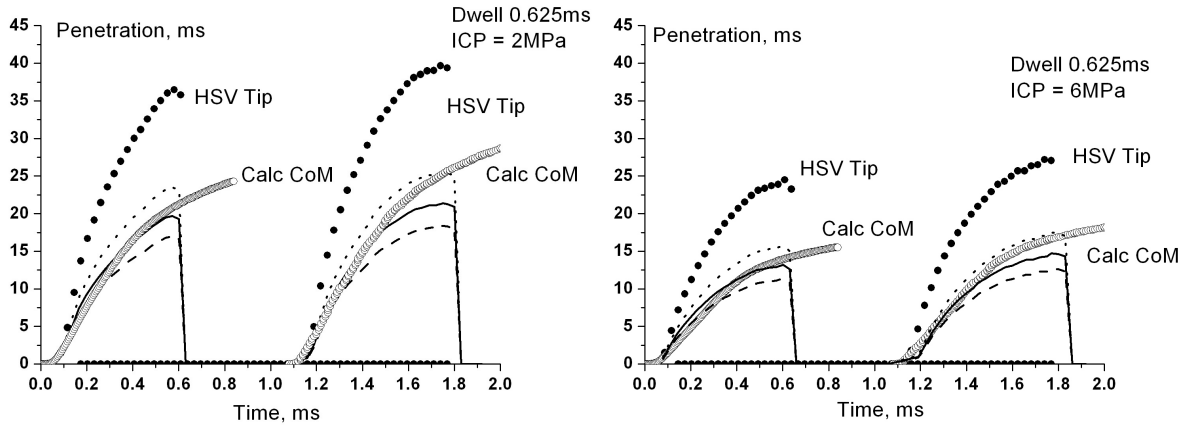

Fig 8a, b. Comparison between calculated and experimental results for the same operating conditions as in Fig 7 except the dwell time 0.625ms.

Conclusions

- An extensive body of the experimental data by laser diagnostics on *Proteus* RCM of ICEG is obtained and analysed in the paper. The results show a good agreement between various experimental techniques giving credibility to the experimental data. This invites their application for benchmarking against available models of spray formation and penetration.
- A model based on the conservation of mass and momentum of the whole spray as a physical body is suggested. The model tracks the position of the centre-of-mass (CoM) of the injected fuel for each split.
- The CoM model is shown to produce a good agreement with the experimental results with the same values of modelling parameters for two values of in-cylinder pressures, ICP = 2MPa and ICP = 6MPa, and two values of dwell between the individual injections in a cycle (splits), 0.425ms and 0.625ms.
- For CFD implementation, the Lagrangian tracking algorithm for dense sprays may be improved by taking into account the direct contribution of neighbouring droplets into the drag force acting on a droplet. This is the subject of work in progress.

Acknowledgements

The authors are grateful to the European Regional Development Fund Franco-British INTERREG III (Project Ref 162/025/247) and EPSRC CASE for New Academics award for partial financial support of the work described in this paper. The authors thank the EPSRC Engineering Instrument Loan Pool for supplying the high-speed video camera. Contribution of Dr G De Sercey for imaging software customisation is gratefully acknowledged.

References

[1]. Arai M. and Amagai K. "Dynamic Behaviour of Multi-Stage Injection Diesel Spray, SAE 97004, 1997
[2]. Baniasad M. S. "Analysis of the fuel injection rate in Diesel injection systems". PhD thesis, University of London, 1994.
[3]. Bosch W. "The Fuel Rate Indicator: A New Measuring Instrument for Display of the Characteristics of Individual Injection", SAE 660749, 1996
[4]. Crua C (2002) Combustion Processes in a Diesel Engine. PhD thesis, December 2002, University of Brighton.
[5]. Karimi K. *et al,* "Development in Diesel Spray Characterisation and Modelling', *Thiesel 2006* Conference on Thermofluid Dynamic Processes in Diesel Engines, Valencia, Spain, 2006
[6]. Kennaird D A. *et al.* In-Cylinder Penetration and Breakup of Diesel Sprays Using a Common Rail Injection System. SAE 2002-01-1626, 2002.
[7]. Lee C.S., Park S.W. "An experimental and Numerical Study on Fuel Atomization Characteristics of High-Pressure Diesel Injection sprays", *Fuel*, p 2417-2423, 2002
[8]. Levich G. V. "Physicochemical hydrodynamics", Prentice-Hall, Inc. Englewood Cliffs, NY, p 639-650, 1962
[9]. Liu A.B. and Reitz R.D. "Mechanism of air-assisted liquid atomisation". Atomization and Spray, Vol. 3, pp. 55-75, (1993).
[10]. Lucas, "Rate of injection manual; High T/P rate gauge manual"; issued 11/9/95.
[11]. Mulholland J.A *et al*."Influence of droplet spacing on drag coefficient in nonevaporating monodisperse streams"AIAA Journal, Vol. 26, No. 10, 1988.
[12]. Pierpont D.A. *et al* "Reducing Particle and NOx Using Multiple Injection and EGR in a Diesel ", SAE950217, 1995
[13]. Sazhin S.S. *et al.* "The initial stage of fuel spray penetration", *Fuel* 82, 875-885, 2003.
[14]. Sazhin S.S. *et al* "A model for fuel spray penetration", *Fuel* 80 2171 – 2180, 2001
[15]. Sazhina E.M. *et al.* "A detailed modelling of the spray ignition process in Diesel engines", *Comb Sci and Technology*, 160, 317-344, 2000
[16]. Tow T.C. *et al,* "Reducing Particulate and NOx Emissions by Using Multiple Injections in a Heavy Duty Diesel Engine", SAE940897, 1994